Capturing Data From Three-Dimensional Surfaces Using Fuzzy Landmarks

CHRISTOPHER J. VALERI,[1] THEODORE M. COLE III,[1,3]
SUBHASH LELE,[2] AND JOAN T. RICHTSMEIER[1]*
[1]*Department of Cell Biology and Anatomy, The Johns Hopkins
University School of Medicine, Baltimore, Maryland*
[2]*Department of Biostatistics, The Johns Hopkins University,
School of Hygiene and Public Health, Baltimore, Maryland*
[3]*Department of Basic Medical Science, School of Medicine,
University of Missouri, Kansas City, Missouri*

ABSTRACT   Anatomical landmarks are defined as biologically meaningful loci that can be unambiguously defined and repeatedly located with a high degree of accuracy and precision. The neurocranial surface is characteristically void of such loci. We define a new class of landmarks, termed fuzzy landmarks, that will allow us to represent the form of the neurocranium. A fuzzy landmark represents the position of a biological structure that is precisely delineated, but occupies an area that is larger than a single point in the observer's reference system. In this study, we present a test case in which the cranial bosses are evaluated as fuzzy landmarks. Five fuzzy landmarks (the cranial bosses) and three traditional landmarks were placed repeatedly by a single observer on three-dimensional (3D) computed tomography (CT) surface reconstructions of pediatric dry skulls and skulls of pediatric patients, and directly on four of the same dry skulls using a 3Space digitizer. Thirty landmark digitizing trials from CT scans show an average error of 1.15 mm local to each fuzzy landmark, while the average error for the last ten trials was 0.75 mm, suggesting a learning curve. Data collected with the 3Space digitizer was comparable. Measurement error of fuzzy landmarks is larger than that of traditional landmarks, but is acceptable, especially since fuzzy landmarks allow inclusion of areas that would otherwise go unsampled. The information obtained is valuable in growth studies, clinical evaluation, and volume measurements. Our method of fuzzy landmarking is not limited to cranial bosses, and can be applied to any other anatomical features with fuzzy boundaries. Am J Phys Anthropol 107:113–124, 1998.   © 1998 Wiley-Liss, Inc.

Anatomical landmarks are defined as biologically meaningful loci that can be unambiguously defined and repeatedly located with a high degree of accuracy and precision (Richtsmeier et al., 1995). Traditional anatomical landmarks include foramina for neurovascular bundles (e.g., foramen spinosum, foramen ovale), the intersection of sutures (e.g., nasion, bregma), and bony processes (e.g., jugular notch, anterior clinoid process). Particular landmarks are chosen based on prior biological knowledge that can help to identify features that have direct bearing on a research question.

A group of landmarks defined on a form provides a repeatable, geometric representation of certain features, but preserves the geometry of a form only partially. Information pertaining to surfaces and outlines is lost when landmarks are used to define a form (Roth, 1993, Read and Lestrel, 1986). If the landmarks are chosen judiciously, the use of landmark data can assure the investigator of homology of the biological structures between individuals, or within an individual over time (Richtsmeier and Lele, 1993).

There are instances where landmarks are disproportionately distributed over a biological object because certain anatomical regions are void of features (Lele and Richtsmeier, 1990). One method for including information from these regions is by the placement of constructed landmarks (Moyers and Bookstein, 1979). Constructed landmarks use geometric combinations of other existing landmarks, along with lines erected at specified angles to "construct" a new landmark. Unfortunately, the homology found in the original landmarks may not be conveyed to the constructed landmark (Bookstein et al., 1985; Rohlf and Bookstein, 1990).

All definitions of landmarks and landmark classes (Bookstein, 1990; Roth, 1993) share the concept of landmark as a point location. Areas that are void of single-point features but have observable, distinct topographic characteristics have been used as landmarks, but only with reference to an arbitrary coordinate system. These landmarks are called "extremal points." For example, glabella is defined as *the most anterior projecting* point of the anterior surface of the frontal bone in the midline (Bass, 1971). The location of this point changes with the exact orientation of the skull. The Frankfurt horizontal plane is conventionally (though not necessarily) used, but even slight variation in orientation can result in a shift in the placement of glabella. Moreover, many extremal points are defined by projecting a 3D form onto a 2D plane.

Areas that are void of single-point features, but have topographic characteristics that *do not* require a coordinate system for definition, exist on many biological objects. By repeatedly locating the apparent centroid of these features and statistically measuring the mean and the variance around the centroid, a new landmark can be established if the variance is acceptably small. We call this new landmark type a "fuzzy landmark." A fuzzy landmark represents a biological structure that is precisely delineated and that corresponds to a locus of some biological significance, but occupies an area that is larger than a single point. Fuzzy landmarks differ from extremal points and constructed points in that the feature we aim to record occupies more than a single point in space and that feature can be identified without locational data from additional landmarks. Our goal is to determine whether or not the position of such features can be represented accurately and repeatedly as a single point.

The potential uses of fuzzy landmarks include studies of growth and development, phylogenetic relationships, heterochrony, allometry, paleoanthropology, and functional morphology. We recently demonstrated the potential importance of fuzzy landmark data in a study of the dysmorphology associated with premature sagittal synostosis (Richtsmeier et al., 1998). In that study, the relative position of the parietal bosses were the primary data points differentiating normal from abnormal morphology. Because the bosses represent the site of the original tubers or ossification centers, we were able to propose an etiological hypothesis regarding sagittal synostosis on the basis of the analysis of the fuzzy landmark data. This is a single example of the use of fuzzy landmark data. Any problem that requires measurement of biological form can benefit from the inclusion of fuzzy landmarks.

Fuzzy landmarks can take many forms. Examples include features of articular surfaces of bones, loci of muscle attachments on bone, undulations and tuberosities on the carapaces of crustaceans, and soft tissue bulges or dimples. This study presents our analysis of the measurement error involved in data collection for five fuzzy landmarks: the parietal, occipital, and frontal bosses (Fig. 1). Our method for determining measurement error is applicable to other biological applications where fuzzy landmarks are needed.
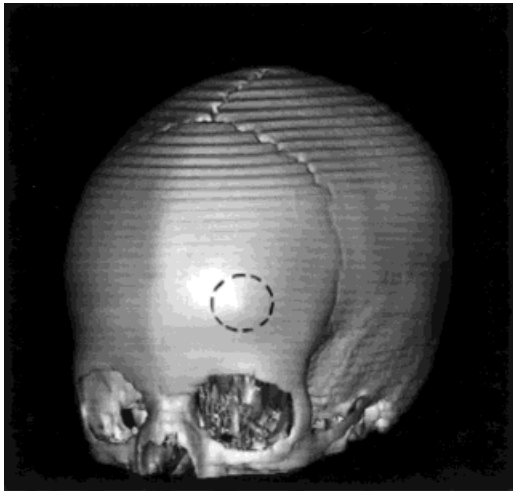
Fig. 1. 3D reconstruction of a CT scan depicting the left frontal boss. As mentioned in the text, the user must define the centroid of the boss and repeatedly locate it with adequate time between trials. The area inside the dotted line represents the area of the boss.

MATERIALS AND METHODS

Landmark data from the 3Space digitizer

Four dry skulls were chosen from the Bosma collection of pediatric dry skulls (Shapiro and Richtsmeier, 1997). The 3D coordinates for five fuzzy landmarks and two traditional landmarks were located on the skulls by one of the authors (CJV) using the Polhemus 3Space tabletop digitizer (Polhemus, Colchester, VT) that has undergone validation (Hildebolt and Vannier, 1988) and precision testing (Corner et al., 1992). Traditional and fuzzy landmarks were collected from these skulls to allow comparison between the two landmark types, since measurement error distributions are known for traditional landmarks (Corner et al., 1992; Richtsmeier et al., 1995). The landmarks included are listed in Table 1 and shown in Figure 2. Landmark 8 (left anterior clinoid process) was not collected using the tabletop digitizer because it lies inside the skull.

Each skull was positioned on the digitizer and fixed in place using plasticine to inhibit movement. The consistent orientation of a single skull for all measurement sessions enabled the use of a statistical model (see below) for within-skull measurement error. Landmark data were collected twice daily:

TABLE 1. Landmark identification: abbreviation and description

Landmark number	Landmark name	Landmark abbreviation	Landmark definition
1	Right frontal boss	RFBOSS	Apex of the frontal boss, right side
2	Left frontal boss	LFBOSS	Apex of the frontal boss, left side
3	Right parietal boss	RPBOSS	Apex of the parietal boss, right side
4	Left parietal boss	LPBOSS	Apex of the parietal boss, left side
5	Occipital boss	OBOSS	Apex of the occipital boss
6	Right fronto-zygomatic junction	RFZJ	Intersection of the frontal and zygomatic bones on the orbital rim
7	Lambda	LAMBDA	Intersection of the sagittal and lambdoid sutures
8*	Left anterior clinoid, process	LACP	Most posterior projecting point of the left anterior clinoid process

* Landmark 8 was only collected from the CT data.

once at the beginning of the day, and once at the end of the day. At least 7 hours elapsed between landmarking sessions to prevent memory-biased placement. Data were collected from each of the skulls 15 times. Skulls were never moved on the digitizer tabletop during this time and were not removed from the digitizer until all landmarking trials were completed.

Landmark data from computed tomography scans

Computed tomography (CT) scans of ten skulls were used for this portion of the study. All scans were obtained using a GE CT9800 scanner housed in the Department of Neuroradiology, The Johns Hopkins Hospital. Six of the scans came from a database of patients that were initially suspected of having craniosynostosis, but were later diagnosed as normal. These scans were produced
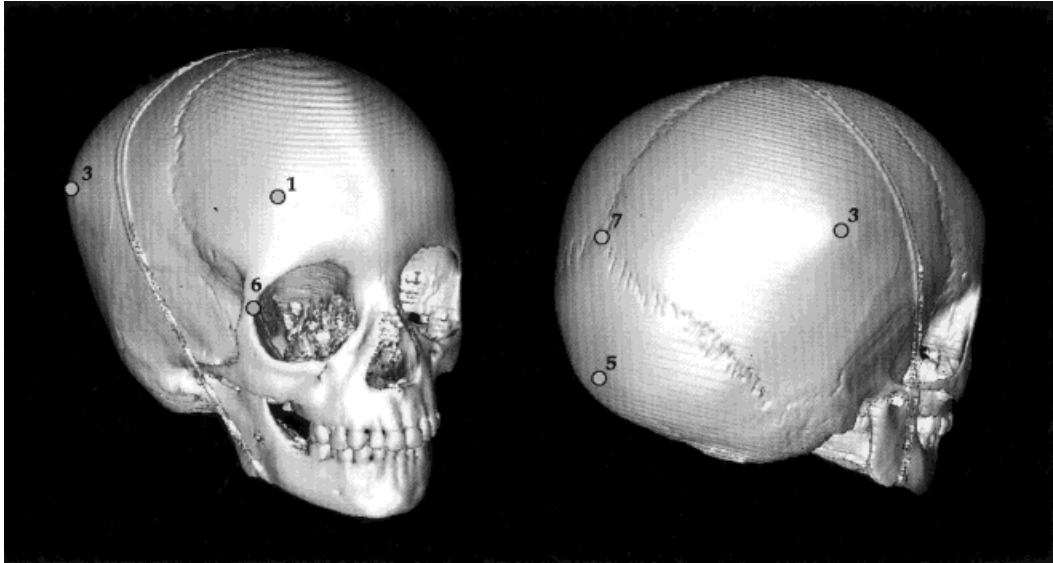
Fig. 2.   Location of landmarks used in this study. The oblique frontal view at left shows landmarks 1, 3, and 6. The oblique parietal view at right shows landmarks 3, 5, and 7. Landmark numbers are defined in Table 1.

using the standard Pediatric Neuroradiology CT scanning protocol of the Johns Hopkins Medical Institutions (parameters vary depending on age/size of patient, slice thickness is constant at 3.0 mm). The four skulls from the Bosma collection that were digitized using the 3Space digitizer were scanned using a research CT scanning protocol (DFOV 21 cm; kV 120; mA 120; slice thickness 1.5 mm). Age of patients is known. Age of the skulls was estimated from tooth eruption patterns following Ubelaker (1989). Five of the subjects (dry skulls and patient data combined) used in this study were less than 1 year of age at the time of the scanning, while the other five ranged from 2–5 years. Four of the patients scanned were males, while the other two were females. The sexes of the dry skulls are unknown.

At the time of CT image acquisition, the Z axis is determined on the basis of a calibrated table movement and the relative location of the successive slice images. The X and Y axes are also established at the time of scanning and represent the rows and columns of pixels within a slice image. Once a 3D reconstruction is created from the slice images, it can be manipulated (translated, rotated, and scaled) by the computer in 3D

space, but the local coordinate system (created during image acquisition) remains internally consistent regardless of the orientation of the reconstruction.

Landmark data were collected from the scans using Remedi (Rendering and Analysis of Medical Images, Center for Information-Enhanced Medicine, National University of Singapore). Remedi allows the visualization of axial slice images, two reconstructed orthogonal views (sagittal and coronal), a 3D surface reconstruction, and the placement of landmarks on any of these views. The digitally stored CT scans are loaded into Remedi and a volume consisting of all axial slice images is created. A 3D-rendered surface can be extracted by selecting a specific bone density. The density measure is calculated on a scale that is defined from zero to 4,000. The lowest value is zero, and the higher the value chosen (lower density), the less bone that is visible in the reconstruction. When a density is chosen, a 3D surface is extracted corresponding to the chosen density value.

Remedi provides many viewing options. For example, the surface can be viewed at any angle, the lighting can be adjusted, and partial surfaces can be visualized. Land-

marks can either be placed on the original axial slice data, one of the two orthogonal views, or directly on the 3D surface created by Remedi.

In addition to the seven landmarks located on each skull using the 3Space digitizer, the left anterior clinoid process was located on the CT data using Remedi (see Table 1, Fig. 2). During each data collection episode, the eight landmarks were digitized on a skull and the 3D coordinates were written to a computer file. Then the CT scan of another specimen was visualized, the eight landmarks were located on that skull, and their coordinates written to a file. This process was repeated for all ten skulls. The data collection sequence was then restarted. Data were collected in this manner in order to erase from the researcher's memory the placement of any landmark on any particular skull in the previous data collection episode. At most, three data collection episodes were completed in one day. Usually, the episodes were separated by one week. In total, the eight landmarks were collected from each CT reconstruction 40 times.

Most traditional landmarks can be seen and digitized from many angles, and can usually be found directly on the axial slice image without the aid of a 3D surface reconstruction. Fuzzy landmarks are less distinct and therefore take more care in placement. After experimenting with many different methods for identifying these landmarks, we concluded that it is best to locate the bosses directly on the 3D reconstruction, with the observer's view being perpendicular to the apex or centroid of the boss. This allows the observer to move the light source, revealing topographic indications that help define an area on the reconstruction that surrounds the apex of the boss. The apex or centroid of this area is recorded as the fuzzy landmark.

Specification of the statistical model

The statistical model for describing measurement error follows Corner et al. (1992) and is presented with specific reference to this study in the Appendix. Briefly, we want to estimate the variability of a fuzzy landmark due solely to locating that landmark on a specimen. We do this by calculating an estimate of the mean and the variance from the various data collection episodes of a single specimen. Because each specimen remains stationary throughout data collection, we can calculate the necessary estimates without using superimposition. We provide an estimate of the mean location of the landmarks in 3D space ($\hat{M}_{ij}$), a variance covariance matrix ($\hat{\Sigma}$) that estimates the error of each landmark along each axis (diagonal elements) along with the covariation in measurement error between landmarks along the X, Y and Z axis (off-diagonal elements), and a matrix ($\hat{\Sigma}$) that estimates the general variation local to a specific landmark without reference to the X, Y, or Z axes. These estimates are calculated separately for each skull and correspond solely to measurement error. The estimates do not include biological variability of landmark location among the various forms we measure.

RESULTS

Landmarks were collected from each 3D CT reconstruction 30 times. Chronologically ordered subsets of 10 digitizing episodes were analyzed separately to investigate the possibility of a learning curve. There was a large amount of variance among the first 10 (1–10) trials, but not in the next 10 trials (11–20). There are two possible explanations for this result: either the observer remembered the location of the bosses from previous landmarking sessions, or the observer's skill at locating the fuzzy landmarks improved over time. Since the landmarking episodes were usually one week apart, and our observer was a novice at landmarking, we favor the latter explanation: the ability to place fuzzy landmarks improves with time. To prevent the learning curve from falsely inflating our measurement error estimates, the first 10 trials (1–10) were removed and replaced with 10 additional trials (31–40). There were 40 trials total, but only the last 30 are reported in the final analysis. The last 10 trials (31–40) had generally lower variance compared to the 30 trial subset (11–40) (see Tables 2 and 3).

Tables 2 and 3 contain the standard deviation of the placement of the landmarks collected using Remedi. These values are

TABLE 2. *Standard deviation (mm) of landmark coordinates[1] for all skulls; Last Ten Trials (trials 31–40)*

Specimens	Landmarks							
	RFBOSS	LFBOSS	RPBOSS	LPBOSS	OBOSS	RFZJ	LAMBDA	LACP
Patient 1	1.04	0.88	0.72	0.81	1.29	0.80	0.30	0.17
Patient 2	0.99	1.24	0.96	1.13	0.56	0.14	0.33	0.14
Patient 3	0.66	0.64	0.71	0.94	0.51	0.20	0.20	0.10
Patient 4	0.99	1.03	0.88	0.64	0.70	0.10	0.26	0.49
Patient 5	0.88	0.65	1.31	0.92	0.50	0.39	0.58	0.10
Patient 6	1.12	1.08	0.90	0.66	0.54	0.17	0.35	0.30
Dry Skull 1	1.13	1.06	0.62	0.50	0.51	0.20	0.32	0.10
Dry Skull 2[2]	0.49	0.54	0.24	0.44	0.93	0.24	0.14	0.14
Dry Skull 3[2]	0.37	0.52	0.28	0.20	0.59	0.26	0.14	0.10
Dry Skull 4	1.11	1.31	0.36	0.65	0.39	0.17	0.26	0.22
Average	**0.88**	**0.90**	**0.70**	**0.69**	**0.65**	**0.27**	**0.29**	**0.19**

[1] These statistics are the square roots of the diagonal elements of $\hat{\Sigma}_K$ (see Appendix) for each skull. Data collected from CT data using Remedi.
[2] Perinatal skull.

TABLE 3. *Standard deviation (mm) of landmark coordinates[1] for all skulls; Thirty Trials (trials 11–40)*

Specimens	Landmarks							
	RFBOSS	LFBOSS	RPBOSS	LPBOSS	OBOSS	RFZJ	LAMBDA	LACP
Patient 1	1.54	1.33	1.09	0.90	1.83	0.59	0.33	0.22
Patient 2	1.39	1.62	1.04	1.17	0.69	0.17	0.35	0.20
Patient 3	1.42	1.13	0.87	1.15	0.62	0.24	0.24	0.14
Patient 4	1.47	1.54	1.77	1.21	1.36	0.17	0.24	0.59
Patient 5	1.46	1.46	1.81	1.07	0.73	0.56	0.97	0.10
Patient 6	1.79	1.64	1.26	1.12	0.71	0.20	0.39	0.30
Dry Skull 1	1.52	1.48	0.72	0.65	0.62	0.28	0.33	0.17
Dry Skull 2[2]	0.81	0.81	0.51	0.72	1.39	0.22	0.14	0.10
Dry Skull 3[2]	1.46	1.20	0.40	0.33	1.18	0.32	0.20	0.14
Dry Skull 4	1.48	1.54	0.82	0.97	0.49	0.22	0.49	0.20
Average	**1.43**	**1.38**	**1.03**	**0.93**	**0.96**	**0.30**	**0.37**	**0.22**

[1] These statistics are the square roots of the diagonal elements of $\hat{\Sigma}_K$ (see Appendix) for each skull. Data collected from CT data using Remedi.
[2] Perinatal skull.

the square roots of the diagonal elements of $\hat{\Sigma}_\kappa$ for each skull. The average error (across skulls *and* landmarks) for locating the fuzzy landmarks in 30 trials (11–40) is 1.15 mm, while the average error in the last 10 trials (31–40) is 0.75 mm. The results suggest that the experience of the observer will influence the number of trials needed.

Our data for 30 trials (Table 3) show that, of the fuzzy landmarks, the least error was seen in locating the parietal and the occipital bosses. The error was greater for the frontal bosses. This is probably due to the more pronounced curvature of the parietal and occipital bones. The parietal bone at the boss is more pointed than the frontal boss. The distributions of the 30 landmarking trials on the CT reconstructions are given in Figure 3.

Variation in landmark placement along the *X*-, *Y*-, and *Z*-axes (*X* = mediolateral, *Y* = anteroposterior, *Z* = superoinferior) was calculated, within-specimen, for each landmark in the last 10 (31–40) trials subset (Table 4). Here, we are concerned with the square roots of the diagonal elements of Σ (see Appendix) for each skull. Maintaining a skull in a single orientation during data collection using the digitizer, or capturing a form on image(s) for collection of data, enables the calculation of error for each specimen using this model. Differences in orientation between specimens precludes us from calculating an average for this type of error across specimens. We provide the error data for two cases separately, first for patient 2 and then for dry skull 4 (Table 4). Table 4 demonstrates the error in three dimensions (*X* = mediolateral , *Y* = superoinferior, *Z* = anteroposterior). These two cases are representative of all others, whether data were
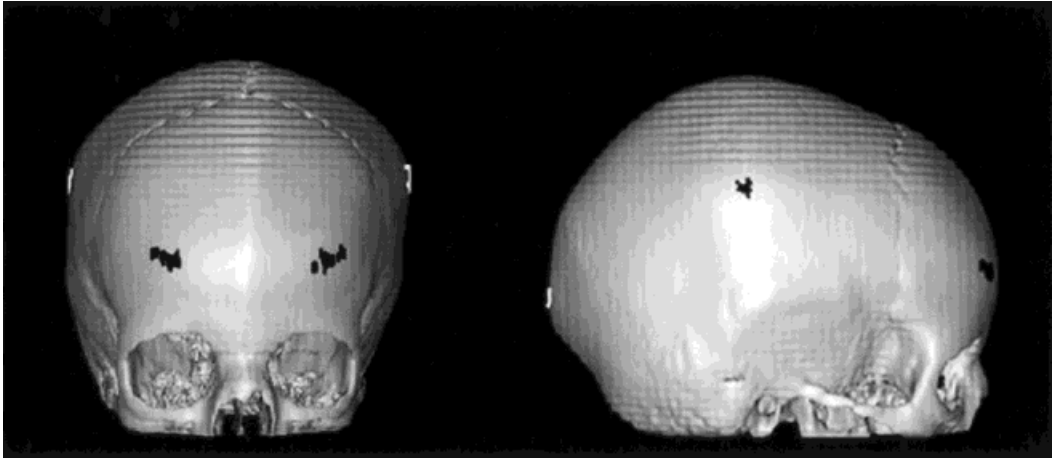
Fig. 3. A visualization of 30 trials of fuzzy landmarks. The frontal view at left shows the right and left frontal bosses in black and the parietal bosses in white. The lateral view at right shows the parietal and frontal bosses in black and a partial representation (along the Z axis) of the occipital boss in white.

TABLE 4. *Error along each axis calculated within specimen using standard deviations (mm) of landmark coordinates[1] from CT data gathered with Remedi (trials 11–40)*

	Patient 2			Dry skull 4		
	X^2	Y^3	Z^4	X	Y	Z
RFBOSS	1.22	0.67	1.01	1.37	0.79	1.11
LFBOSS	1.56	0.85	1.20	1.66	1.00	1.18
RPBOSS	0.17	0.95	1.35	0.12	0.42	0.45
LPBOSS	0.17	1.19	1.55	0.15	0.84	0.74
OBOSS	0.51	0.00	0.82	0.34	0.01	0.59
RFZJ	0.10	0.10	0.14	0.18	0.13	0.20
LAMBDA	0.35	0.40	0.22	0.22	0.27	0.28
LACP	0.14	0.17	0.14	0.36	0.13	0.02

[1] These statistics are the square roots of the diagonal elements of Σ for each skull. This measurement error is presented for single specimens and therefore does not include biological variability.
[2] X = mediolateral.
[3] Y = anteroposterior.
[4] Z = superoinferior.

collected directly from the form using the digitizer or from CT images.

At each boss, the spatial distribution of the repeated digitizations resembles a parabolic surface. Like the actual skull surface, the surface of the 3D reconstruction defines and disproportionately limits the location of a landmark in one direction, so little error is expected in the direction orthogonal to the skull surface. Our results follow our expectations. For the frontal bosses, the error was largest in the X (mediolateral) and Z (superoinferior) axes. Relatively little error is seen in the Y (anteroposterior) axis. This is because variation in the Y axis would result

in a landmark either floating anterior to the surface or embedded in the surface. Similar error distributions can be seen for the other two bosses. Relatively increased error was recorded in the Y and Z axes for the parietal bosses. The X axis lies orthogonal to the surface for the parietal bosses. The occipital boss error is almost completely limited to the X and Z axes. Little error occurs along the Y axis for the occipital boss, as the surface lies orthogonal to the Y axis.

Our measurement error for traditional landmarks are comparatively reduced (Tables 2 and 3) and are consistent with previous measurement error studies (Corner et al., 1992). There is little difference in error between the 30 trial (11–40) and the last 10 (31–40) trial subsets for the traditional landmarks, suggesting the lack of a learning curve for the traditional landmarks—most likely because they are represented by single points.

Coordinate location data for fuzzy landmarks using the 3Space digitizer (Table 5) is comparable to the data collected using Remedi for the last 10 trials (Table 2). Comparison between CT data (Table 2) and 3Space data (Table 5) collected from the perinatal skulls (dry skulls 2 and 3) show similar error. For older pediatric specimens (dry skulls 1 and 4 (both approximately 4 years old)), the error in data collected using the

TABLE 5. *Standard deviation (mm) in seven landmarks[1] calculated from dry skulls using the 3Space tabletop digitizer (15 trials)*

Specimen	Landmarks						
	RFBOSS	LFBOSS	RPBOSS	LPBOSS	OBOSS	RFZJ	LAMBDA
Dry Skull 1	0.95	1.32	1.09	1.00	1.77	0.32	0.22
Dry Skull 2[2]	0.63	0.72	0.62	0.42	1.04	0.24	0.42
Dry Skull 3[2]	0.71	0.78	0.55	0.56	0.60	0.35	0.30
Dry Skull 4	0.71	1.33	1.53	1.44	1.37	0.61	0.35

[1] These statistics are the square roots of the diagonal elements of $\hat{\Sigma}_K$ for each skull.
[2] Perinatal skull.

TABLE 6. *Error along each axis calculated within specimen using standard deviations (mm) of landmark coordinates[1] gathered with the 3Space tabletop digitizer (15 trials)*

	Dry skull 4		
	X	Y	Z
RFBOSS	0.66	0.56	0.89
LFBOSS	1.05	1.67	1.17
RPBOSS	1.70	0.83	1.86
LPBOSS	1.40	0.23	2.06
OBOSS	0.84	1.91	1.14
RFZJ	0.45	0.63	0.71
LAMBDA	0.34	0.38	0.29

[1] These statistics are the square roots of the diagonal elements of Σ for each skull. This measurement error does not include a measure of biological variability.

3Space digitizer (Table 5) is greater than the CT data (Table 2). There appeared to be no learning curve for locating the fuzzy landmarks on the 3Space digitizer. This could be because the observer had experienced the learning curve while locating the cranial bosses using Remedi, because the bosses are more easily seen directly on the skull, or because less training is required with the digitizer.

DISCUSSION

A method for locating the frontal and parietal bosses on CT axial slice data has been proposed and validated by Mathijssen et al. (1996). In their model, the bosses were marked on dry skulls with small pieces of clay. The marked skulls were CT-scanned and the 2D coordinates of the clay were recorded as the location of the bosses from axial slice images. The sharpest angle on each bone (the boss) was also located on the axial CT slices. Mathijssen et al. (1996) place the bosses on the CT slice chosen on the basis of alternate structures (slice transecting the most anterolateral points of the lateral ventricles and the occiput above the inion) following Waitzman et al. (1992). The mean difference between the clay and the sharpest angle was 0.3 mm. Because the boss was located on a fixed CT slice, error along the superoinferior axis (choice of the slice) was ignored.

In our study, the cranial bosses are recognized as 3D structures, and data are collected accordingly. We consider error along all three axes. Also, we explicitly recognize the neurocranial bosses as small regions and collect landmark data to estimate the centroids. This approach requires that we estimate an average location from repeated trials of locating the landmark.

When data are collected using the digitizer, any movement of a skull between trials results in a change in the local coordinate system. Movement of the skull prevents consistent estimation of an average location for each landmark and of the variation local to the landmark, because there is no preferred registration between different coordinate systems and, therefore, no correct way to superimpose the trials (Lele, 1993; Lele and McCulloch, 1998; Rao and Suryawanshi, 1996).

Our research suggests that when locating fuzzy landmarks it is important to view the desired landmark location from many different perspectives to assure the closest placement to the desired location. The 3Space digitizer allows the observer to move around the object and to physically feel the fuzzy location, but since the study design requires that the skull be fixed, there are physical constraints on the ability of a person to view various aspects of the skull. Remedi does not allow the user to palpate the boss, but it does enable the viewer access to the specimen from any of 360° of rotation around the specimen.

Fig. 4. Comparison of an infant skull to the skull of a child. Note the shapes of the bosses. On the infant skull the bosses are very pointed, allowing very accurate location of the bosses.

Fuzzy landmarking of the cranial bosses is shown to have acceptable error, especially in younger skulls where the bosses are more pronounced. Repeated measurements of dry skulls 2 and 3 (Table 2) have less variance than the others (with the exception of the occipital boss). These specimens are both perinatal skulls. The bosses are more pronounced on a younger skull (Fig. 4), and therefore they can be placed with more accuracy. A general negative correlation between precision in landmarking the neurocranial bosses and the age of the specimen is predicted from our observations on this small sample. This prediction, which is specific to our study, may have general implications for other studies. If the feature being recorded as a fuzzy landmark is one that varies with respect to other biological influences (e.g., sex, age, locomotory preferences, or phylogenetic association) measurement error may vary according to these associations. These observations should be considered at the time of measurement error analysis, as they may have profound effects on the results of biological analyses.

For every study, the investigator must determine what constitutes acceptable error. Pilot data should be collected and analyzed in subsets to determine the number of trials necessary for minimizing error. In our study, the fuzzy landmarks were defined because we lacked data from the neurocranial surface. Our chosen analytical technique, Euclidean Distance Matrix Analysis (Lele, 1991, 1993; Lele and Richtsmeier, 1991, 1995), uses all possible linear distances calculated from the landmarks in analysis. Since the fuzzy landmarks are located on a surface void of traditional landmarks, and this surface is relatively isolated from surrounding structures, linear distances that have a fuzzy landmark as an endpoint will be relatively long. For example, even our largest errors (Table 3) would constitute less than 3% of a linear distance 6.5 cm in length (average distance from right fronto-zygomatic junction to right frontal boss).

This study does not report interobserver error, although that work is in progress. Because fuzzy landmarks are defined by the observer who is placing them, there is the possibility that interobserver error will be increased. We suggest that laboratories that have multiple persons involved in data collection should conduct both intra- and interobserver error studies.

We stress that our results are specific to the cranial bosses, but the general characteristics of fuzzy landmarks and the methods for determining the measurement error involved in their identification are broadly applicable. Our method can be used for other anatomical features that have fuzzy boundaries. However, every new fuzzy landmark must undergo an error study similar to the one used in this article. The acceptable degree of error is variable, depending on the overall isolation of the feature that is being landmarked and the goals of the study.

ACKNOWLEDGMENTS

LITERATURE CITED

Bass W (1971) Human Osteology: A Laboratory and Field Manual of the Human Skeleton. Columbia, MO: Missouri Archeological Society.

Bookstein F (1990) Introduction to methods for landmark data. In FJ Rohlf and FL Bookstein (eds): Proceedings of the Michigan Morphometrics Workshop. Ann Arbor: University of Michigan Museum of Zoology, pp. 215–225.

Bookstein F, Chernoff B, Elder R, Humphries J, Smith G, and Strauss R (1985) Morphometrics in evolutionary biology. Philadelphia: Academy of Natural Sciences.

Corner BD, Lele S, and Richtsmeier JT (1992) Measuring precision of three-dimensional landmark data. J Quant Anthropol 3:347–359.

Hildebolt C, and Vannier M (1988) Three-dimensional measurement accuracy of skull surface landmarks. Am J Phys Anthropol 76:497–504.

Lele S (1991) Some comments on coordinate free and scale invariant methods in morphometrics. Am J Phys Anthropol 85:407–418.

Lele S (1993) Euclidean distance matrix analysis (EDMA) of landmark data: estimation of mean form and mean form difference. Math Geol 25:573–602.

Lele S, and McCulloch C (1998) Invariance and morphometrics. J Am Stat Assoc (submitted).

Lele S, and Richtsmeier J (1990) Statistical models in morphometrics: Are they realistic? Syst Zool 39: 60–69.

Lele S, and Richtsmeier JT (1991) Euclidean distance matrix analysis: A coordinate free approach to comparing biological shapes using landmark data. Am J Phys Anthropol 98:73–86.

Lele S, and Richtsmeier J (1995) Euclidean distance matrix analysis: Confidence intervals for form and growth differences. Am J Phys Anthropol 98:73–86.

Mathijssen MJ, Vaandrager JM, van der Meulen JC, Pieterman H, Zonneveld FW, Kreiborg S, and Vermeij-Keers C (1996) The role of bone centers in the pathogenesis of craniosynostosis: An embryologic approach using CT measurements in isolated craniosynostosis and Apert and Crouzon syndromes. Plast Reconstruct Surg 98:17–26.

Moyers RE, and Bookstein FL (1979) The inappropriateness of conventional cephalometrics. Am J Orthodont 75:599–617.

Rao C, and Suryawanshi S (1996) Statistical analysis of shape of objects based on landmark data. Proc Natl Acad Sci USA 93:12132–12136.

Read D, and Lestrel P (1986) Comment on uses of homologous-point measures in systematics: A reply to Bookstein et al. Syst Zool 35:241–253.

Richtsmeier JT, and Lele S (1993) A coordinate-free approach to the analysis of growth patterns: Models and theoretical considerations. Biol Rev 68:381–411.

Richtsmeier J, Paik C, Elfert P, Cole TM, and Dahlman H (1995) Precision, repeatability and validation of the localization of cranial landmarks using computed tomography scans. Cleft Palate Craniofac J 32: 217–227.

Richtsmeier JT, Cole TM III, Krovitz G, Valeri CJ, and Lele S (1998) Preoperative morphology and development in sagittal synostosis. J Craniofac Gen Dev Biol 18:64–78.

Rohlf FJ, and Bookstein FL, (1990) Proceedings of the Michigan Morphometrics Workshop. Ann Arbor: University of Michigan Museum of Zoology.

Roth V (1993) On three-dimensional morphometrics, and on the identification of landmark points. In L Marcus, E Bello, A Garcia-Valdecasas (eds): Contributions to Morphometrics. Madrid: Museo Nacional de Ciencias Naturales, CSIC, pp. 41–61.

Shapiro D, and Richtsmeier J (1997) Brief communication: A sample of pediatric skulls available for study. Am J Phys Anthropol 103:415–416.

Ubelaker DH (1989) Human Skeletal Remains: Excavation, Analysis, Interpretation. Washington, DC: Taraxacum

Waitzman AA, Posnick JC, Armstrong DC, and Pron GE (1992) Craniofacial skeletal measurements based on computed tomography. II. Normal values and growth trends. Cleft Palate Craniofac J 29:118–127.

APPENDIX

Suppose we measure the form of a single skull repeatedly by recording K 3D landmarks n times. For the data collected using the 3Space digitizer, $K = 7$, while $K = 8$ for the data collected from CT scans. The coordinates for the mth of n measurement trials is represented by a $K \times 3$ matrix called $\mathbf{T_m}$:

$$
T_m = \begin{bmatrix}
T_{1X,m} & T_{1Y,m} & T_{1Z,m} \\
T_{2X,m} & T_{2Y,m} & T_{2Z,m} \\
\vdots & \vdots & \vdots \\
T_{KX,m} & T_{KY,m} & T_{KZ,m}
\end{bmatrix}
$$

so that each row of the matrix corresponds to a particular landmark, while each column corresponds to an axis in the local coordinate system. For example, $\mathbf{T}_{1X,m}$ is the x-coordinate value for landmark 1 on the mth trial.

The first step in describing measurement error is to compute the mean locations of the K landmarks for the n trials. Because our research design requires that the skull is held stationary with respect to the local coordinate system (by fixing the skull to the digitizer for the dry skulls and because a coordinate system is defined when a CT scan is done), computation of the maximum-likelihood estimate of the mean within a specimen is straightforward:

$$
\hat{M} = \frac{1}{n} \sum_{m=1}^{n} T_m
$$

In other words, we compute the mean estimate by simply taking the element-wise means of the repeated measurements across the n trials, so that $\hat{M}$ has the same dimensions ($K \times 3$) as each of the $\mathbf{T}$ matrices. Note

that superimposition or "fitting" of the coordinates from the n different trials is not required, because the skull remains stationary (i.e., the coordinate system is constant across trials).

The next step is to describe the amount of variation local to each landmark. One way of describing variation in a landmark is to compute variances that are specific to each of the axes in the local coordinate system. For example, we may ask, "What is the variation in the location of the right parietal boss along the X-axis?" Similar questions can be posed for each of the landmarks and each of the coordinate-system axes. All of the information needed for answering these questions is contained in a variance-covariance matrix called Σ. Σ is a square and symmetric matrix, with K times D rows and columns. In the case of the 3Space data, Σ is 21×21, while Σ is 24×24 for the CT data. The structure of Σ is most clearly illustrated by dividing it into submatrices, as follows:

$$\Sigma = \begin{bmatrix} \Sigma_{XX} & \Sigma_{XY} & \Sigma_{XZ} \\ \Sigma_{XY} & \Sigma_{YY} & \Sigma_{YZ} \\ \Sigma_{XZ} & \Sigma_{YZ} & \Sigma_{ZZ} \end{bmatrix}$$

where each Σ_{XX}, Σ_{XY}, etc., are submatrices of $K \times K$ dimensions (7×7 or 8×8, in our cases), and each row and column within a submatrix is associated with a landmark. The subscripts of the submatrices indicate which of the axes in the local coordinate system are represented. For example, the submatrix Σ_{XX} has the following structure:

$$\Sigma_{XX} = \begin{bmatrix} \mathrm{var}(1X) & \cdots & \cdots & \mathrm{cov}(1X,KX) \\ \mathrm{cov}(2X,1X) & \mathrm{var}(2X) & \cdots & \cdots \\ \cdots & \cdots & \cdots & \cdots \\ \mathrm{cov}(KX,1X) & \cdots & \cdots & \mathrm{var}(KX) \end{bmatrix}$$

where the numbers in parentheses are landmark and axis identifiers. Thus, var(1X) is the variability around landmark 1 in the X-axis direction. The diagonal elements of Σ_{XX} represent the variances of the land-

marks along the X-axis, while the off-diagonals measure landmark covariances along that same axis. Relatively small variances indicate landmarks that can be measured with high repeatability, whereas larger variances indicate landmarks that are more susceptible to measurement error. The other diagonal *submatrices* of Σ (i.e., Σ_{YY} and Σ_{ZZ}) have similar structures, and their diagonal elements have similar interpretations. The off-diagonal submatrices (Σ_{XY}, Σ_{XZ}, and Σ_{YZ}) describe covariances among measurement errors along the different coordinate-system axes. We expect that the X-, Y-, and Z-axis components are independently distributed, both within and between landmarks, so that all of the elements in the off-diagonal submatrices should be near zero.

Because each skull remains stationary through all of the n trials, we can obtain a maximum-likelihood estimate of Σ, which we call $\hat{\Sigma}$, corresponding to each skull. The first step in the computation is to mean-center the coordinates for each trial by element-wise subtraction of the mean coordinates:

$$\hat{X}_m^C = T_m - \hat{M}$$

We then rewrite each $K \times 3$ matrix $\hat{X}_m^C$ in the form of a vector:

$$\mathrm{vec}(\hat{X}_m^C)$$

$$= \left[\hat{X}_{1X,m}^C \cdots \hat{X}_{8X,m}^C \; \hat{X}_{1Y,m}^C \cdots \hat{X}_{8Y,m}^C \; \hat{X}_{1Z,m}^C \cdots \hat{X}_{8Z,m}^C \right]^T$$

where T denotes a transpose. In our case, each vector has either 21 (3Space digitizer data with 7 landmarks) or 24 (CT scan with 8 landmarks) elements. The estimate of $\hat{\epsilon}$ is then

$$\hat{\epsilon} = \frac{1}{n} \sum_{m=1}^{n} \left\{ \left[\mathrm{vec}(\hat{X}_m^C) \right] \left[\mathrm{vec}(\hat{X}_m^C) \right]^T \right\}$$

The dimensions of $\hat{\epsilon}$ are 21×21 and 24×24 for the 3Space and CT data, respectively. Again, we are interested only in interpreting the diagonal elements of the matrix.

We may also compute a smaller ($K \times K$) matrix that describes variation in and among the landmarks *in general*, without reference to the axes of the local coordinate system. Following Lele (1993), we call this matrix

ϵ_κ, with the corresponding maximum-likelihood estimate $\hat{\epsilon}_\kappa$:

$$\hat{\epsilon}_\kappa = \frac{1}{3n} \sum_{m=1}^{n} (\hat{X}_m^c)(\hat{X}_m^c)^T$$

Note that $\hat{X}_m^c$ is a $K \times D$ matrix. Each of the diagonal elements of $\hat{\epsilon}_\kappa$ describes the variation in a single landmark location. These are more general descriptions of variation because they contain information about all of the coordinate-system axes simultaneously.

The magnitudes of the diagonal elements are proportional to the amount of measurement error. Highly repeatable landmarks will have variances that are closer to zero, while the variances of more error-prone landmarks will be relatively larger. $\hat{\epsilon}_\kappa$ and $\hat{\epsilon}$ are calculated separately for each skull. Consequently, these estimates correspond solely to measurement error and do not confound the biological variability of landmark location among the various forms we measure.